Enhanced electron-phonon coupling at the Au/Mo(112) surface

Keisuke Fukutani,[1] Hirokazu Hayashi,[2] Ivan N. Yakovkin,[3] Takafumi Habuchi,[2] Daisuke Hirayama,[2] Jian Jiang,[4] Hideaki Iwasawa,[4] Kenya Shimada,[4] Ya. B. Losovyj,[1] and Peter A. Dowben[1]

[1]*Department of Physics and Astronomy, Jorgensen Hall, P.O. Box 880299, University of Nebraska-Lincoln, Lincoln, Nebraska 68588-0299, USA*

[2]*Graduate School of Science, Hiroshima University, 1-3-1 Kagamiyama, Higashi-Hiroshima, Hiroshima 739-8526, Japan*

[3]*Institute of Physics, National Academy of Sciences of Ukraine, Prospect Nauki 46, Kiev, UA 03028, Ukraine*

[4]*Hiroshima Synchrotron Radiation Center, Hiroshima University, 2-313 Kagamiyama, Higashi-Hiroshima, Hiroshima 739-0046, Japan*

(Received 19 September 2012; published 30 November 2012)

A detailed investigation of the electronic structure and electron-phonon coupling for a Au monolayer on the Mo(112) surface is presented. The electronic states of bulk Mo and the (112) surface-derived states are seen to strongly hybridize with those of the Au overlayer, resulting in the formation of surface resonance states localized near the surface and the interface of Au/Mo(112). The experimentally extracted self-energy due to the electron-phonon coupling on one of the surface resonance bands gives a good quantitative agreement with the calculations. The strength of electron-phonon coupling for Au/Mo(112) is discussed in terms of the mass enhancement factor and is considerably larger than for the Mo(112) surface. Such an increase in the mass enhancement factor in the vicinity of the Fermi level likely derives from the soft surface phonon modes created upon Au adsorption.

DOI: 10.1103/PhysRevB.86.205432 PACS number(s): 73.20.At, 73.20.Mf, 63.20.kd

I. INTRODUCTION

Electron-phonon coupling is one of the most fundamental many-body interactions in solid-state physics, and essential for a proper description of many properties of materials as well as critical phenomena in solids.[1] The former includes low-temperature electronic heat capacity and finite electrical conductivity. The latter ranges from surface reconstructions to superconducting phase transitions.[2,3] Although the electron-phonon coupling is ubiquitous, due to the low excitation energy of phonons (typically <100 meV for metals), its effect on the electronic structure is most pronounced in the vicinity of Fermi level (E_F). Therefore, the quantification of electron-phonon coupling is most readily realized in the metallic systems for which the excitation energy is, by definition, zero.

The detailed experimental investigations of electron-phonon coupling using high-resolution angle-resolved photoemission spectroscopy (ARPES) have become more common. Since the first direct experimental quantifications of the electron-phonon coupling in Be(0001)[4] and Mo(110)[5] in 1999, ARPES has been applied to elucidate the nature of electron-phonon coupling in various metals, including Be(0001),[6–8] Cu(111), Ag(111), Au(111),[9–12] Fe(110),[13,14] Al(100),[9,15–17] and Mo(112).[18,19] So far, the characterization of the electron-phonon coupling has been largely limited to clean, adsorbate-free systems, and only a few studies have been devoted to the examinations of the electron-phonon coupling of adsorbate structures, such as H/W(110), for which a noticeable enhancement of the electron-phonon coupling has been observed.[20,21] Yet, adsorbate structures are known to exhibit various types of interesting phenomena such as overlayer structural phase transitions, and thus, major insights in such adlayer phase transitions and properties may be obtained from a quantitative characterization of the electron-phonon coupling in overlayer structures.

The Mo(112) surface is known to exhibit a highly anisotropic electronic structure[22] on which Au forms commensurate atomic chains, as schematically illustrated in Fig. 1(a). At certain coverages of Au/Mo(112), order-disorder transitions of the Au chains have been observed.[23] Electron-phonon coupling may well play an important role in such overlayer instabilities, and thus, our investigation of the electron-phonon coupling of Au/Mo(112) can serve as an important milestone in the study of such overlayer instability.

II. EXPERIMENTAL DETAILS

The high-resolution ARPES was performed at the linear undulator beamline (BL-1)[24] of Hiroshima Synchrotron Radiation Center (HiSOR) at Hiroshima University, Japan. The surface of the Mo(112) sample was cleaned by the standard method of repeated annealing (at $\sim$1400 °C) in oxygen atmosphere with the oxygen partial pressure of $\sim 1 \times 10^{-6}$ torr, followed by cycles of annealing at 1000–1300 °C and flashing at $\sim$1800 °C, similar to the procedures used elsewhere.[22,25–29] Low-energy electron diffraction (LEED) and Auger electron spectroscopy (AES) were used to verify the quality of the Mo(112) surface. The amount of surface contamination, mainly C and O, were evaluated to be below the detection limit of the AES.

Deposition of Au was performed by physical vapor evaporation of Au onto the Mo(112) sample by heating the Au source below the melting temperature. The Au growth rate was adjusted to be sufficiently slow to ensure the layer-by-layer growth on Mo(112) surface up to the coverage of one monolayer (ML), for which the structure is illustrated in Fig. 1(a). The constant gradual growth of Au film within the submonolayer coverage was monitored by the linear relationship between the adsorbate coverage and Au peak intensity in AES.[30] At coverages near the completion of 1 ML, LEED was used to confirm the formation of the 1 ML 1×1 adlayer.

The high-resolution ARPES spectra were taken along the $\bar{\Gamma} - \bar{X}$ line in the $\langle \bar{1}\bar{1}1 \rangle$ direction in the surface Brillouin

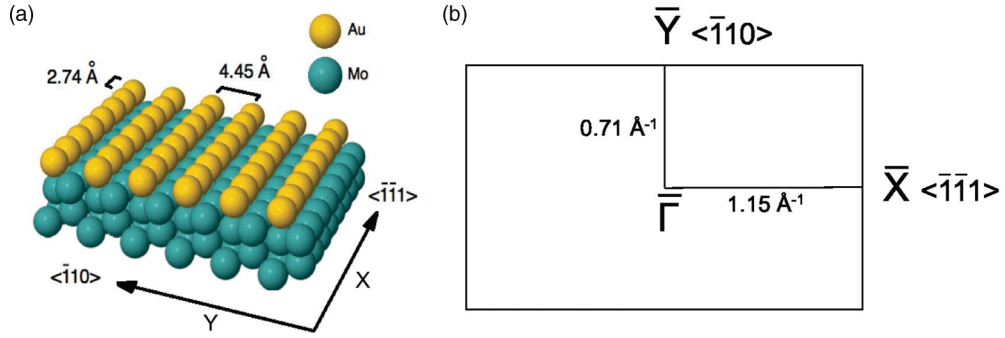

FIG. 1. (Color online) The schematic illustration of Au/Mo(112) at the coverage of nominal 1 ML (a). The corresponding SBZ is illustrated in (b) with the approximate dimensions along the $\bar{\Gamma} - \bar{X}$ and $\bar{\Gamma} - \bar{Y}$ lines.

zone (SBZ), schematically illustrated in Fig. 1(b), with the p polarization geometries [where the vector potential of incident photon **A** lies within the detection plane or xz plane in Fig. 1(a)]. The ARPES experiments were carried out using the angular mode of the hemispherical electron analyzer (R4000, VG Scienta). The experimental band structure mappings for the entire dimension along the $\bar{\Gamma} - \bar{X}$ line (as will be seen in Fig. 2) were performed using the incident photon energy of $\hbar\omega = 22$ eV with the analyzer acceptance angle of $\pm 15^\circ$ (angular 30 mode). The energy resolution was estimated to be 10 meV, and the angular resolution was $\sim 0.9^\circ$, corresponding to the wave-vector resolution of ~ 0.03 Å^{-1} at E_F. The close-up of the surface resonance band near E_F (as will be seen in Fig. 3) was taken with the incident photon energy of $\hbar\omega =$ 22 eV, with the analyzer acceptance angle of $\pm 7^\circ$ (angular 14 mode) and the estimated energy resolution of ~ 10 meV and the angular resolution of $\sim 0.2^\circ$, corresponding to a wave-vector resolution of ~ 0.008 Å^{-1} at E_F. The temperature of the sample was maintained at ~ 60 K by constant flow of liquid helium. Throughout the discussion, the binding energies are referenced to the Fermi level, in terms of E_F–E.

III. THEORETICAL METHODOLOGY

The density functional theory (DFT) semirelativistic calculations included the generalized gradient approximation (GGA),[31] and were performed with the ABINIT[32] package using Troullier-Martins norm-conserving pseudopotentials.[33] The periodicity in the direction normal to the surface was maintained by adopting the repeat-slab model. The slabs were built of seven layers of Mo(112) atomic planes with one Au layer on one side of the slab for the 1-ML Au/Mo(112) system. The vacuum gap was about 10 Å. The optimization of atomic positions was performed until all forces became less than 0.05 eV/Å. The energy cutoff of 20 hartree and $6 \times 4 \times 1$ Monkhorst-Pack set of special k points provided the 0.001 hartree convergence of the total energy.

The phonon band structure, phonon density of states, $F(\omega)$, and the Eliashberg function, $\alpha^2 F(\omega)$, were calculated by the response function method,[34] implemented in the ABINIT set of programs.[32] The isotropic Eliashberg function was obtained by averaging over the wave vectors k_i and k_f of initial and final states on the Fermi surface. Using the Eliashberg function, we calculated the real and imaginary parts of the self-energy due to the electron-phonon coupling, and compared with the experimental ones in Sec. V.

IV. ELECTRONIC STRUCTURE OF Au/Mo(112)

Prior to the investigation of the electron-phonon coupling of Au/Mo(112), its detailed electronic band structure near E_F must be understood. This is crucial in two ways: (1) since the electron-phonon coupling parameters in bulk and in surface are generally different, the origin of the bands (that is to say, whether the band is surface derived, bulk derived or a surface resonance) should be clearly understood when the experimental results are to be compared to the *ab initio* calculation, (2) due to the finite resolution of ARPES, there arises, in some cases, overlap of the spectral intensities that can obscure the small renormalization of the electronic band dispersion.[22] Having the detailed picture of the band structure mapped by ARPES enables us to choose the appropriate band (not obscured by a nearby band) for the accurate characterization of the electron-phonon coupling parameters.

Figure 2(a) shows the experimental band structure of the clean Mo(112) substrate along the $\bar{\Gamma} - \bar{X}$ line obtained by ARPES with the p polarization geometry (after Ref. 22). Among the four bands seen to cross the Fermi level, the bands labeled a_2 ($k_F = 0.60$) and a_4 ($k_F = 0.81$ Å^{-1}) have been identified to be surface derived, while the bands a_1 ($k_F =$ 0.47 Å^{-1}) and a_3 ($k_F = 0.64$ Å^{-1}) are projected bulk bands. As the surface of Mo(112) is covered by Au, the significant change in the band structure is observed. Figure 2(b) shows the ARPES band mapping of Au/Mo(112) at the nominal Au coverage of 1 ML, as schematically illustrated in Fig. 1(a). Note that since the ARPES band mapping in Fig. 2(b) was taken with p polarization geometry (see Sec. II), only the electronic states with even reflection parity with respect to the $\bar{\Gamma} - \bar{X}$ line are observed due to the photoemission selection rules[35] (the initial states with odd reflection parity can be observed with s polarization geometry). As is expected, the adsorption of 1-ML Au results in the significant modification to the surface-derived bands [a_2 and a_4 in Fig. 2(a)] of the Mo(112) substrate. The clean Mo(112) surface-weighted band a_4 [Fig. 2(a)], with $k_F = 0.81$ Å^{-1}, is shifted to larger wave vectors away from the SBZ center to become the band b_4 in Fig. 2(b), observed with $k_F = 0.91$ Å^{-1} for Au/Mo(112). On the other hand, the other surface band of Mo(112), labeled a_2

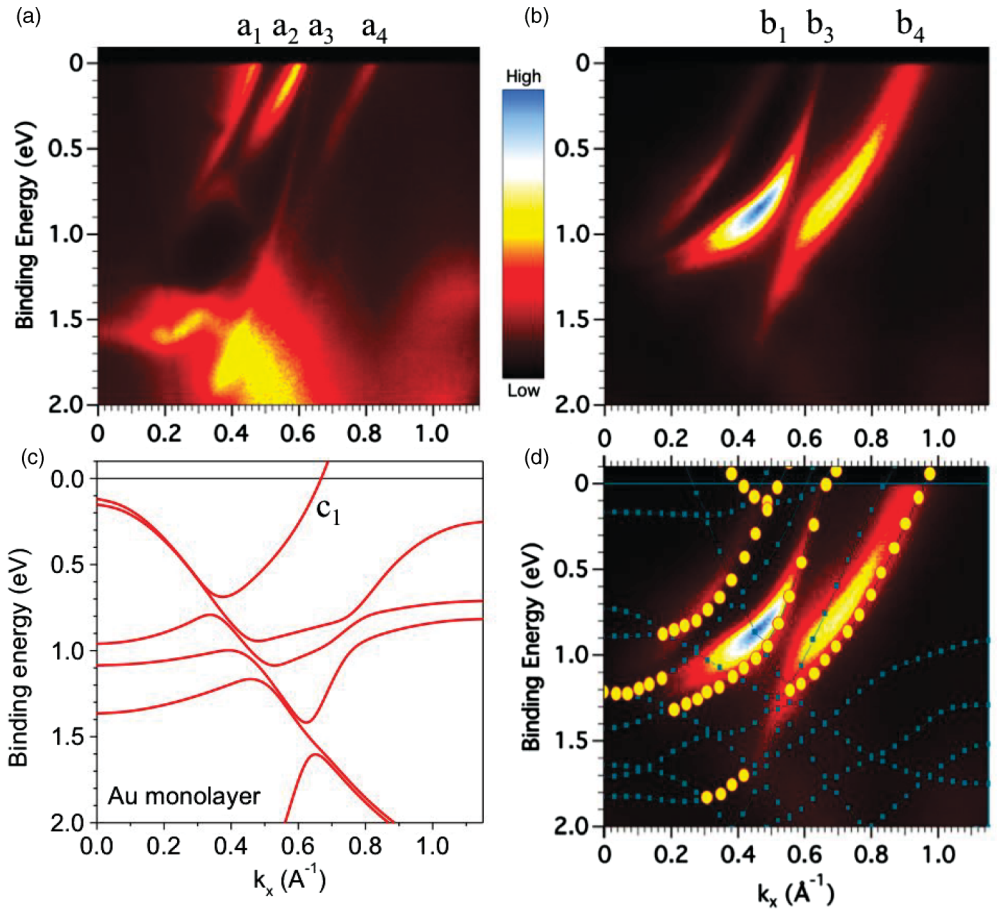

FIG. 2. (Color) The ARPES band mapping taken along the $\bar{\Gamma} - \bar{X}$ line with the incident photon energy of 22 eV with p polarization geometry (i.e., only the states with even reflection parity about $\bar{\Gamma} - \bar{X}$ are visible) for (a) Mo(112) (reprinted from Ref. 22) and (b) 1 ML Au/Mo(112). (c) This shows the band structure along the $\bar{\Gamma} - \bar{X}$ line of the free-standing ML of Au with the same structure as the topmost layer of Mo(112). The band with the Fermi-level crossing of $k_F = 0.64$ Å^{-1} can be identified and is expected to hybridize with the Mo bulk state with nearly the same Fermi momentum k_F. The band structure calculated from the seven-layer slab model is overlaid for 1 ML Au/Mo(112) in (d). For (d), the significantly surface-weighted states with even reflection parity are marked with yellow circles.

[Fig. 2(a)], has disappeared from the ARPES spectrum upon Au adsorption [Fig. 2(b)].

The bulk-derived bands are affected less upon Au adsorption. Although the band a_1, a projected Mo bulk band with $k_F = 0.47$ Å^{-1} [Fig. 2(a)], is slightly shifted and ARPES intensity diminishes within 0.5 eV from E_F (relative to the rest portion of the band), the general features of dispersion remain unchanged after the Au adsorption, which is then seen as the band b_1 in Fig. 2(b). The dispersion of the band a_3 (another Mo bulk band with $k_F = 0.64$ Å^{-1}) is more significantly affected by the Au adsorption, which evolves into the band b_3 in Fig. 2(b). This change in the E-k dispersion and the enhancement of the ARPES intensity for the band b_3, near 0.8-eV binding energy, is clearly evident in Fig. 2(b); the E-k dispersion changes sufficiently so that the b_3 band exhibits "bending" that is absent in the band a_3 in clean Mo(112). Thus, it is evident that adsorption of a Au ML results in modification of the band structure of Mo(112) not only for its surface-derived states but also for the projected bulk states.

It is important to note that the modification of the surface potential induced by the Au adsorption should quickly diminish into the bulk of Mo(112) due to the screening in metal substrate, and therefore, the observed change in the projected bulk band structure should not be directly attributed to the change in the surface potential. The noticeable modification in the projected bulk states should, therefore, be derived from the hybridization with the electronic states of the Au overlayer. Consequently, it is plausible to expect that the bands b_1 and b_3, observed with $k_F = 0.51$ and 0.64 Å^{-1}, respectively in Fig. 2(b), are surface resonance bands, which have large weight (i.e., amplitude of the wave function) near the surface but penetrate into the Mo bulk with non-negligible amplitude.

This view is consistent with theoretical expectations. Figure 2(c) shows the calculated band structure of a free-standing Au ML [detached from the Au/Mo(112) surface shown in Fig. 1(a)] plotted along the $\bar{\Gamma} - \bar{X}$ direction. In this plot, the band that crosses the Fermi level at $k_F = 0.64$ Å^{-1}, labeled c_1, is apparent, and it is seen to exhibit nearly parabolic dispersion down to ~500 meV. This Au band (c_1) is expected to hybridize with the Mo bulk band (a_3) to form a surface resonance band upon the adsorption on the Mo(112) surface. This is due to the presence of projected bulk bands of Mo(112),[22] namely, the band a_3 observed in ARPES [Fig. 1(a)], in the region of band c_1 for the free-standing Au ML. Figure 2(d) shows

the calculated surface band structure of 1 ML Au/Mo(112) based on the seven-layer slab model overlaid on the ARPES spectrum of Fig. 2(b). The expected surface resonance band (the result of hybridization of the band c_1 and a_3) appears with $k_F = 0.66$ Å^{-1} and agrees well with the band b_3 observed in ARPES. The band structure calculation for Au/Mo(112) indicates noticeable surface weight for this band (∼52%) as well as for the other two bands seen to cross the Fermi level in ARPES spectrum (i.e., b_1 and b_4).

Here, it must be noted that the band structure calculation indicates the odd reflection parity for the Au band with downward dispersion away from the SBZ center. Therefore, due to known photoemission selection rules,[35] this Au-derived band should only be observed with *s* polarization geometry (or with unpolarized light). This explains the absence of this Au band in the ARPES band mapping taken with *p* polarization geometry [Fig. 2(b)]. Although there are several other Au bands that are not clearly identified in ARPES band mapping in Fig. 2(b), this is perhaps either due to the odd-reflection parities of those states or weak matrix elements in the photoemission process. Nonetheless, it is evident that the band b_3 observed with $k_F = 0.64$ Å^{-1} in ARPES should be identified as the surface resonance band arising from the hybridization between the Au overlayer states and the projected bulk states of Mo(112).

V. ELECTRON-PHONON COUPLING

The central equation in the analysis of electron-phonon coupling as well as other many-body interactions is quasiparticle spectral function (note that for convenience, we set $\hbar = 1$ throughout the following discussion):[36]

$$A(\omega,k;T) = -\frac{1}{\pi}\frac{\Sigma_I(\omega,k;T)}{[\omega - E(k) - \Sigma_R(\omega,k;T)]^2 + \Sigma_I(\omega,k;T)^2}, \tag{1}$$

where Σ_R and Σ_I are, respectively, the real and imaginary part of self-energy ($\Sigma = \Sigma_R + i\Sigma_I$) and $E(k)$ is the dispersion relation for the bare particles (i.e., without many-body interactions). Note that Σ_I is intrinsically a negative quantity. From the experimental perspective, the starting point is the observation of $A(\omega, k)$ by ARPES, and the goal is to find the self-energy associated with electron-phonon coupling. By finding the bare particle dispersion relation $E(k)$ using some method, it is possible to obtain the complex self-energy $\Sigma(\omega, k)$ from the observed spectral function, which characterizes the many-body interactions of the material in question.[5,8,13–18]

In general, the total self-energy (Σ) in Eq. (1) consists of contributions due to electron-phonon coupling [$\Sigma^{(e-p)}$], electron-electron coupling [$\Sigma^{(e-e)}$], and electron-impurity coupling [$\Sigma^{(e-i)}$]. These self-energy contributions are additive, provided that the interaction mechanisms are independent, namely,

$$\Sigma = \Sigma^{(e-p)} + \Sigma^{(e-e)} + \Sigma^{(e-i)}. \tag{2}$$

As the self-energy is a causal complex function, between the real and imaginary part, the Kramers-Kronig relation should hold as

$$\Sigma_R(\omega,k) = \frac{1}{\pi}P\int_{-\infty}^{\infty}\frac{\Sigma_I(\omega',k)}{\omega' - \omega}d\omega', \tag{3}$$

where P denotes the Cauchy principal value. In calculations near the singularity at $\omega' = \omega$ in the Kramers-Kronig transform, $\omega' = \omega \pm 1$ meV was each divided into the increment of 10^{-5} meV to obtain the proper convergence, equivalent to taking the Cauchy principal value numerically.

Besides the self-energy, another quantity of interest is mass enhancement factor at the Fermi level $1 + \lambda(k = k_F; T)$, which is defined by the equation

$$m^*/m = 1 + \lambda(k_F;T), \tag{4a}$$

where m and m^* are the "bare" (or unrenormalized) band mass and the "dressed" (or renormalized) band mass of the electron, respectively. The mass enhancement parameter λ can be related to the real part of self-energy as

$$\lambda(k_F;T) = -\left.\frac{\partial\Sigma_R(\omega,k_F;T)}{\partial\omega}\right|_{\omega=0}. \tag{4b}$$

From a theoretical perspective, the starting point, in assessing band renormalization of the experimental band structure due to electron-phonon coupling, is the calculation of the Eliashberg function $\alpha^2(\omega, k)F(\omega, k)$, and the goal is to obtain the spectral function (or the self-energy). Once the Eliashberg function has been determined, it is possible to calculate the imaginary part of the self-energy due to the electron-phonon coupling using the equation

$$\Sigma_I(\omega,k;T) = -\pi\int_0^{\infty}\alpha^2(\omega',k)F(\omega',k)[1 - f(\omega-\omega';T) + f(\omega+\omega';T) + 2n(\omega';T)]d\omega', \tag{5}$$

where f and n are Fermi and Bose distribution functions, respectively. To obtain the self-energy, the integration of Eq. (5) was performed in the 1-meV step using the midpoint rule. Further decrease in the integration step size was seen to result in negligible alterations to the numerical results. The real part of the self-energy can then be obtained using the Kramers-Kronig relation Eq. (3). If the bare particle dispersion relation $E(k)$ is known, the spectral function can also be obtained with the self-energy.

The difficulty is, of course, in calculating the Eliashberg function, which in the most general case depends on energy ω as well as the wave vector k. The first-principle calculation of the ω- and k-dependent Eliashberg functions is a formidable task, and it is conventional to compute the Eliashberg function averaged over the entire Brillouin zone so that it only depends on ω [i.e., $\alpha^2(\omega)F(\omega)$]. The mass enhancement parameter due to the electron-phonon coupling (or electron-phonon coupling parameter) λ, in the zero-temperature limit, can be obtained as the inverse moment of the Eliashberg function in energy as

$$\lambda(T=0) = \int_0^{\infty}\frac{\alpha^2(\omega)F(\omega)}{\omega}d\omega. \tag{6}$$

There are two physically equivalent methods to extract the self-energy from the observed spectral function. One method is to slice the ARPES spectrum at constant momentum k, which gives the sequence of energy distribution curves (EDCs) for each k. The other method is to slice the ARPES spectrum at

constant energy, which gives the sequence of momentum distribution curves (MDCs). Although, in principle, both methods are equivalent, the MDC method is usually more advantageous. The spectral functions are not precisely Lorentzian either in the EDC or the MDC due to the k dependence and ω dependence of Σ as well as the functional dependence of $E(k)$. However, the k dependence of Σ is negligible in many cases, including the present one compared to the ω dependence in the vicinity of single band. Furthermore, if we make the approximation $E(k) = -v(k - k_F)$ (v = band velocity), justified sufficiently close to E_F, then the MDC line shape is in fact Lorentzian with the peak position (k_{peak}) and full width at half-maximum (Γ) given by

$$\begin{aligned} k_{\text{peak}}(\omega) &= k_F - \frac{1}{v}[\omega - \Sigma_R(\omega)] \\ \Gamma(\omega) &= -\frac{2}{v}\Sigma_I(\omega) \end{aligned} \tag{7}$$

for each MDC with fixed energy ω. Thus, MDC slices are generally expected to fit a Lorentzian line shape better than the EDCs, whose line shape can be strongly asymmetric in ω. For this reason, in the present study, the MDC methods were employed to extract the peak position and the width of the line shape, which directly relates to the real and imaginary part of Σ as in Eq. (7).

The presence of the surface resonance states for Au/Mo(112), resulting from the hybridization of the Mo bulk states with the surface states on the Au overlayer, makes the system ideal for investigating the effect of adsorption on the strength of electron-phonon coupling. So far, several experimental and theoretical studies of Mo[5,18,19,34] have been devoted to the characterization of the electron-phonon coupling parameters of the bulk as well as various surfaces. In particular, the mass enhancement parameter due to the electron-phonon coupling for Mo bulk was calculated to be $\lambda = 0.39$–0.42,[19,34] which may be in agreement with the possible experimental identification of $\lambda = 0.42$ for the bulk-weighted band[18,22] (some of the possible complications are detailed in Ref. 22). The electron-phonon coupling parameters λ for Mo(110) and Mo(112) have also been reported[5,19] and are summarized in Table I. Thus, there are fairly consistent characterizations of the electron-phonon coupling parameters for the Mo substrate.

In this study, the theoretical and experimental investigations of the electron-phonon coupling parameters for 1 ML Au/Mo(112) have been carried out and are compared to those of the clean Mo substrate. Here, the band b_3 with $k_F = 0.64$ Å^{-1} [see Fig. 2(b)] is analyzed with MDC method described above with the energy increment of 1.5 meV to extract the peak positions (k_{peak}) as well as the linewidth (Γ).

TABLE I. Mass enhancement parameters $\lambda(T = 0)$.

	Theory	Experiment
Mo bulk	0.39–0.42[19,34]	0.42[18]
Mo(110)	–	0.42–0.52[5]
Mo(112)	0.46[19]	–
Au/Mo(112)	0.68 (0.67 at 60 K)	0.70 (0.65 at 60 K)

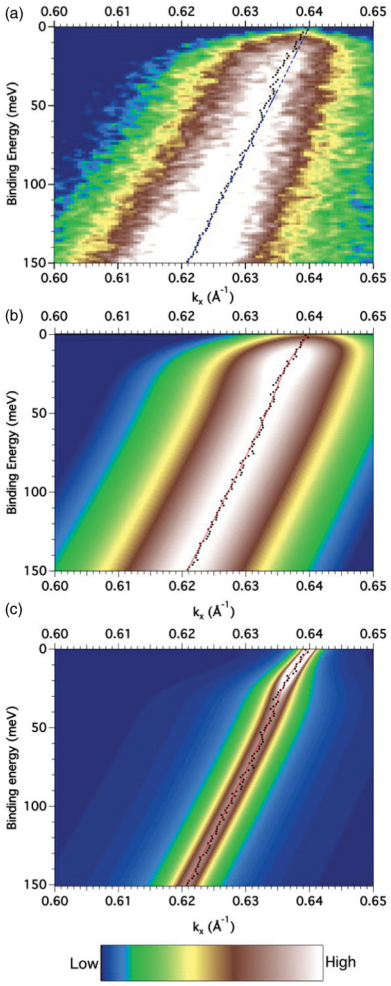

FIG. 3. (Color) (a) The ARPES spectrum taken along the $\bar{\Gamma} - \bar{X}$ line in the vicinity of the Fermi level. The surface resonance band with $k_F = 0.64$ Å^{-1} is seen to exhibit band renormalization (a mass enhancement in the dispersion) due to electron-phonon coupling within ~50 meV below the Fermi level. The peak positions obtained in the MDCs are indicated with circles (●), and the expected unrenormalized band dispersion is indicated with a blue broken curve. (b) The spectral function weighted with the Fermi function at $T = 60$ K in the vicinity of Fermi level calculated from the theoretically determined Eliashberg function and experimentally determined bare band dispersion $E(k)$ and the impurity scattering rate (estimated to be ~78-meV contribution to Σ_I). The experimental MDC peak positions (●), determined from ARPES, are overlaid for the comparison and are seen to agree well with the theoretically expected renormalization. The peaks of the calculated spectral functions are denoted as a red solid curve as a visual guide. (c) The calculated spectral function in which impurity scattering is *turned off* (band renormalization is solely due to electron-phonon coupling). The agreement between the ARPES-determined MDC peak positions (●) and the calculated band distortion is more apparent. Note that the change to the Fermi edge cutoff at finite temperature (60 K) is also turned off for the visual clarity.

Figure 3(a) shows the ARPES spectrum of the analyzed b3/c1 band within 150 meV from E_F. The MDC peak positions as well as the expected bare dispersion (broken curve fitted by parabola with the fixed k_F determined from the experiment)

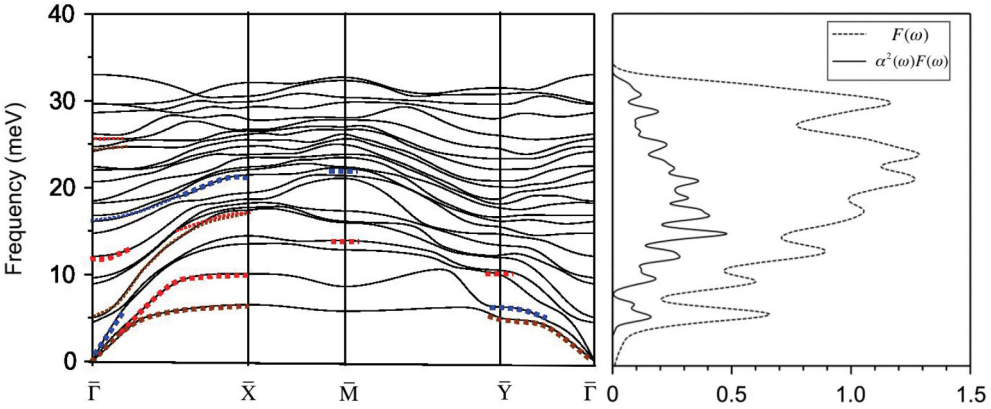

FIG. 4. (Color) The phonon band structure calculated using the seven-layer slab model is shown in (a), where the surface-weighted modes are marked with a thick dotted line (blue = longitudinal mode; red = vertical mode; brown = horizontal mode). The isotropic Eliashberg function, $\alpha^2 F(\omega)$, calculated from the seven-layer slab model is shown in (b). Note that the Eliashberg function is dimensionless.

are overlaid. The distortion of the band within ∼50 meV below E_F, characteristic of the electron-phonon coupling, is apparent. The parabolic fit shows an excellent match down to at least 500 meV and is given by

$$E(k) = -17.666k^2 + 14.404k - 1.9828, \qquad (8)$$

where E and k are measured in units of electron volts and per Ångstrom, respectively.

Figure 4 shows the calculated phonon density of states $F(\omega)$ and the phonon band structure. The electron-phonon coupling function $\alpha^2(\omega)$ have been calculated as outlined in Sec. III, and give the Eliashberg function $\alpha^2(\omega)F(\omega)$ shown as the solid curve in Fig. 4. Given the Eliashberg function, the spectral function can be calculated using the experimentally determined bare dispersion $E(k)$ given by Eq. (8) and the broadening due to the electron-impurity coupling (whose value is estimated below), as shown in Fig. 3(b). The calculated MDC peak positions are shown as a solid curve. In the simulation [Fig. 3(b)], the finite energy resolution and the self-energy due to the electron-electron coupling were not included. As described below, the electron-electron coupling is not significant near E_F. In Fig. 3(b), the experimental MDC peak positions are also indicated and are in good agreement with the calculated spectral function. Figure 3(c) shows the calculated spectral function with electron-impurity coupling "turned off"; the agreement between the experimental MDC peak positions and the expected characteristic distortion [of band b_3 in Fig. 2(b)] due to electron-phonon coupling is more clearly seen.

In order to get further quantitative insights into the self-energy resulting from electron-phonon coupling, the experimental self-energy was extracted using Eq. (7) with the group velocity $v = -35.332k + 14.404$ eV/Å^{-1} and may be compared to the calculated self-energy at $T = 60$ K (solid curves), as in Fig. 5. It can be seen that for the real part of the self-energy [Fig. 5(a)], there is reasonable agreement between theory and experiment (note that in the binding energy scale as employed here, Σ_R is negative for the occupied states). Figure 5(b) also illustrates good agreement between theory and experiment for the imaginary part of the self-energy, provided that the calculated Σ_I is rigidly shifted up by 171 meV, corresponding to the electron-impurity coupling and the instrumental broadening of the MDC linewidth. Since the MCD width at E_F is evaluated to be ∼0.022 Å^{-1} and the instrumental angular resolution is estimated to be 0.2° (or in k space ∼0.008 Å^{-1}), the broadening due to the electron-impurity coupling can be estimated as ∼0.019 Å^{-1}. Thus, the self-energy contribution from the electron-impurity coupling can be estimated as $2\Sigma_I^{(e-i)} \sim 156$ meV. Note that the electron-impurity coupling only affects the lifetime of the quasiparticle, and hence $\Sigma_R^{(e-i)} = 0$, while the electron-impurity coupling gives a Lorentzian line shape and the instrumental broadening is modeled by a Gaussian line shape.

It is important to mention that since the Au band, which is the focus of much of our attention here, is a surface resonance, the hybridization of the local (surface) state of Au [band c_1 in Fig. 2(c)] with the Mo bulk continuum [band a_3 in Fig. 2(a)] may cause the linewidth broadening. However, given the agreement of the experimental and calculated self-energy due to electron-phonon coupling and the internal consistency between experimental Σ_R and Σ_I [related by Kramers-Kronig relation Eq. (3)], the linewidth broadening due to such Au-Mo hybridization is either negligible or nearly constant within the small window of 150 meV below E_F. Thus, some portion of the estimated $2\Sigma_I^{(e-i)} \sim$ 156 meV may be due to the bulk-surface hybridization. Note that the real part of self-energy due to hybridization is already accounted for in the "unrenormalized" parabolic fit in Fig. 3(a) and thus expected to give negligible alteration in Fig. 5(a).

Another scattering mechanism, electron-electron coupling is expected to give rise to the self-energy $\Sigma^{(e-e)}$ with the monotonic increase in $|2\Sigma_I^{(e-e)}|$ as a function of binding energy[15,37,38] and has been observed in various metallic systems, including Mo.[18] For Au/Mo(112), as can be seen from the essentially constant imaginary part ($2\Sigma_I \sim 210$ meV for $E > 50$ meV) in Fig. 5(b), $\Sigma^{(e-e)}$ appears to be dominated by $\Sigma^{(e-p)}$ and $\Sigma^{(e-i)}$, and the contribution from $\Sigma^{(e-e)}$ is likely rather small, in contrast to the situation that applies to the Mo substrate.[18]

From the point of view of anisotropy of the system, it is rather surprising that the experimentally extracted $\Sigma^{(e-p)}$ for a specific band gives a good agreement with that calculated by averaging over all the possible k_i and k_f. Such a calculation gives identical $\Sigma^{(e-p)}$ values for all the bands in the

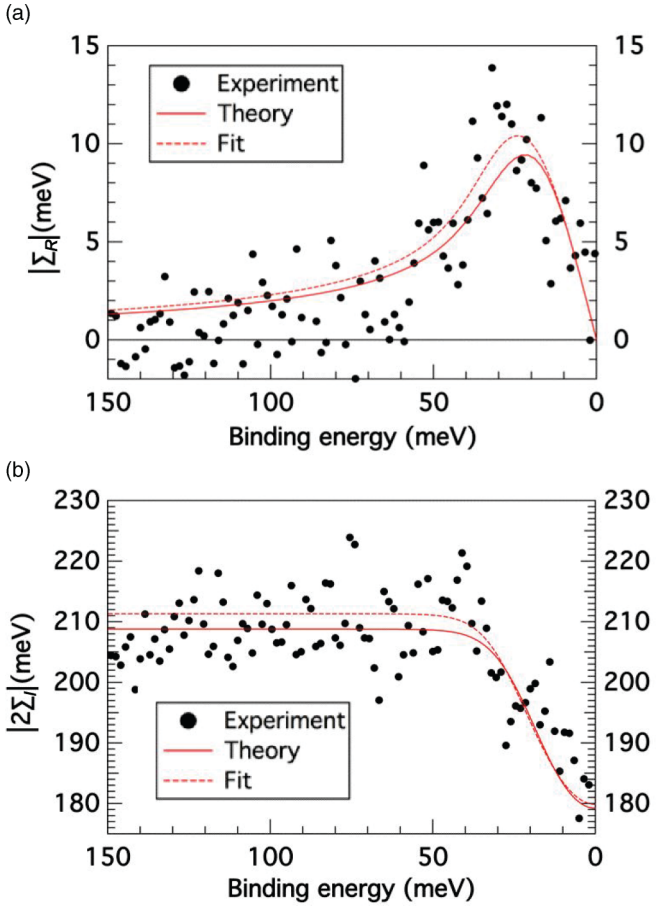

FIG. 5. (Color online) The plots of the real part (a), and the imaginary part (b) of self-energy for the surface resonance band with $k_F = 0.64$ Å^{-1}. The experimental data points (●) for Σ_R are obtained from the deviation of the ARPES peak positions from the expected unrenormalized band dispersion [see Fig. 3(a)], and those for Σ_I are obtained from the width of the photoemission peaks as described in the text. The calculated self-energy due to electron-phonon coupling was obtained using Eqs. (3) and (5), from the calculated isotropic Eliashberg function at $T = 60$ K and plotted as solid curves. The calculated Σ_I is rigidly shifted up by 171 meV, so as to fit the experimental data (interpreted as deriving from the electron-impurity coupling and instrumental broadening as discussed in text). The dotted curves represent the self-energy obtained from the free-parameter Eliashberg function that gives the best fit to the experimental data.

entire SBZ, whereas, in general, it should be different for each band. Either the structural and electronic anisotropy of 1 ML Au/Mo(112) is not significant enough to cause major anisotropy in electron-phonon coupling (to the degree it can be readily identified on the scale of Fig. 5) or the band chosen for this particular analysis "coincidentally" agrees very well with the homogeneous (or averaged) model of electron-phonon coupling, in spite of the anisotropic electronic structure.[22]

VI. THE IMPORTANT PHONON MODES FOR ELECTRON-PHONON COUPLING

Given the evidence in favor of electron-phonon coupling near the interface of Au/Mo(112), it is worthwhile to explore qualitatively the important modes for electron-phonon coupling [i.e., which phonon modes may be giving rise to the major contribution to $\Sigma^{(e-p)}$] for the observed band b_3 with ($k_F = 0.64$ Å^{-1}). Note that the low-energy phonon modes contribute more significantly to the self-energy than those lying at higher energy. This can be seen from the fact that the electron-phonon coupling matrix element is proportional to $\omega^{-1/2}$ [see (A5) in the Appendix]. In fact, it has been pointed out that the contributions from the acoustic phonon modes (or Rayleigh modes) give dominant contribution to the electron-phonon coupling at the surface of Cu(111), Ag(111), and Au(111).[9,10] In Fig. 4, among the surface phonon modes accessible along the $\bar{\Gamma} - \bar{X}$ line (marked by colored squares), the surface acoustic modes (shear horizontal modes in brown and vertical modes in red) lie well below the bulk band edge and produce the pronounced peaks at 5 and 9 meV in the phonon density of states $F(\omega)$. However, along the $\bar{\Gamma} - \bar{X}$ line, the symmetry of the electronic states and the phonon modes restricts the possible modes available for electron-phonon coupling. Since the electronic states and phonon modes lying along $\bar{\Gamma} - \bar{X}$ are described by the C_{1h} group, they can be classified as either even (A′ irreducible representation) or odd (A″) with respect to the reflection about the $\bar{\Gamma} - \bar{X}$ line. Since experimental band mapping in Fig. 2(b) as well as Fig. 3(a) is taken with p polarization geometry, in which the vector potential of the incident light lies within xz plane [see Fig. 1(a)], according to the dipole selection rule,[35] the electronic bands analyzed for the electron-phonon coupling is of even symmetry (A′). On the other hand, the symmetry properties of phonons are classified by their polarizations. It can be derived for the group of C_{1h}, under certain reasonable approximations, that the electron-phonon coupling matrix element vanishes unless the electronic state and phonon mode are both even or both odd (the detailed derivations are summarized in the Appendix). Thus, the shear horizontal phonon modes (marked brown) are forbidden to couple with the electrons in the Au overlayer band that has been the focus of much of our analysis here. Although this selection rule is valid only along the $\bar{\Gamma} - \bar{X}$ line, the coupling matrix element is usually small near this high-symmetry line if present at all. One can therefore expect that shear horizontal modes contribute less to the observed self-energy than do the shear vertical modes. This leads to the inference that the surface phonons, particularly shear vertical modes, play an important role in the observed electron-phonon coupling in addition to whatever may be the contribution from the bulk phonons.

VII. THE ENHANCEMENT OF ELECTRON-PHONON COUPLING

The mass enhancement parameter $\lambda(T)$, as defined in Eq. (4), is important in characterizing the electron-phonon coupling strength. In the present study, λ estimated from the calculated Eliashberg function gives $\lambda(T = 0) = 0.68$ and $\lambda(T = 60\,\text{K}) = 0.67$. The experimental extraction of $\lambda(T)$ involves some difficulty as the slope of $\Sigma_R^{(e-p)}(\omega)$, with respect to ω, must be evaluated right at E_F, in the energy region around which the ARPES intensity diminishes proportional to the Fermi function. In order to overcome this difficulty, we have fit the experimental $\Sigma_R(\omega)$ using the free-parameter

Eliashberg function $\alpha^2 F(\omega)$, in which α^2 is taken to be the energy-independent free parameter, and extract λ associated with the $\alpha^2 F(\omega)$, which gives the best fit for both $\Sigma_R(\omega)$ and $\Sigma_I(\omega)$.

The dotted curves in Fig. 5 shows the self-energy extracted from the free-parameter Eliashberg function with $\alpha^2 = 0.23$. This fit gives a better overall match with the experimental data points [particularly for $\Sigma_R(\omega)$]. Given this free-parameter Eliashberg function, the λ can be estimated as 0.70 at $T = 0$ and 0.65 at $T = 60$ K, providing fairly good agreement between the theory and the experiment. This is consistent with the overall agreement between the theory and the experiment obtained for the mass enhancement parameter λ, as summarized in Table I.

The λ of 1 ML Au/Mo(112) should now be compared to that of the Mo substrate. Although the combination of theory and experiment gives the range of $\lambda = 0.68$–0.70, it is evidently larger than $\lambda = 0.39$–0.42 for Mo bulk and $\lambda = 0.42$ for Mo(112) surface as identified in the previous studies (see Table I). It is plausible to argue that *adsorption of Au on Mo(112) enhances the electron-phonon coupling*. Such an increase in λ can be viewed as a direct consequence of the soft Au phonon modes contributions to the electron-phonon coupling. Thus, the addition of soft phonon modes by means of adsorption does affect the electron-phonon coupling parameter and the quasiparticle effective mass.

VIII. SUMMARY

The investigation of the electronic structure and the electron-phonon coupling parameters of Au/Mo(112), at a nominal adlayer coverage of 1 ML of Au, has been performed by means of high-resolution ARPES and DFT calculations. The adsorption of Au modifies the electronic band structure of Mo(112), and the details of the band structure indicate that the hybridization occurs between the projected bulk electronic states of Mo(112) and those of the Au overlayer. The detailed analysis of the ARPES spectrum leads to evaluations of the many-body interactions in terms of electron-phonon, electron-electron, and electron-impurity coupling near the interface of Au/Mo(112) and suggests that the electron-phonon coupling provides a dominant contribution to the self-energy of quasiparticles. In spite of the appreciable structural and electronic anisotropy of Au/Mo(112), the DFT calculation of the k-averaged Eliashberg function yields a self-energy due to electron-phonon coupling in good agreement with experiment, in spite of the flaws of applying a k-averaged Eliashberg function to a particular k point along the $\bar{\Gamma} - \bar{X}$ Brillouin zone line. Given the change in the quasiparticle self-energy upon Au adsorption on Mo(112), the Au overlayer enhances the strength of electron-phonon coupling at E_F (from 0.39–0.42 to 0.68–0.70) and noticeably suppresses the electron-electron interaction. The enhancement of electron-phonon coupling likely derives from the creation of soft surface phonon modes upon Au adsorption.

ACKNOWLEDGMENTS

This work was partially supported by the IMI Program of the National Science Foundation under Award No. DMR 0843934 and the UNL NSF "QSPINS" MRSEC (DMR-0820521). The authors acknowledge Koji Miyamoto at HiSOR for technical assistance and valuable discussions and James K. Glasbrenner for computational assistance. The experiments have been done under the approval of HiSOR (Proposal No. 10-B-32).

APPENDIX: SELECTION RULE FOR ELECTRON-PHONON COUPLING

The matrix element that describes the electron-phonon coupling is given by[1,39]

$$\langle \alpha', \beta' | H_{\rm ep} | \alpha, \beta \rangle, \tag{A1}$$

where $H_{\rm ep}$ is the electron-phonon coupling Hamiltonian and α (α') and β (β') denote the complete set of quantum numbers for initial (final) electron state and phonon state, respectively. In the rigid-ion approximation,[1,39] $H_{\rm ep}$ can be written in position basis as

$$H_{\rm ep} = \sum_j u_j \cdot \nabla V(r - R_j), \tag{A2}$$

where u_j is the small displacement of jth ion from its equilibrium position R_j. Assuming the electronic part of the wave function can be written as a product of Bloch states, the coupling of a single electron with wave vector k with phonon mode of wave vector q and polarization p can be described by the matrix element

$$M_{\rm ep} = \langle \beta' | \int \psi^*_{k'} \sum_j u_j \cdot \nabla V(r - R_j)\, \psi_k d^3 r | \beta \rangle, \tag{A3}$$

where ψ_k and $\psi_{k'}$ denote the initial and final electronic wave functions, respectively. Since the displacement u_j is an operator that acts on the phonon states,

$$u_j = -i \sum_{q,p} \left(\frac{\hbar}{2NM\omega_{q,p}} \right)^{1/2} e^{iq \cdot R_j} (a^+_{q,p} + a_{-q,p}) \hat{p}, \tag{A4}$$

where $a^+_{q,p}$ and $a_{-q,p}$ are the creation and annihilation operators of the phonon with wave vector q and polarization p, respectively, and $\hat{p}$ is the phonon polarization unit vector. The matrix element becomes

$$\begin{aligned} M_{\rm ep} = \sum_j \langle \beta' | - i \sum_{q,p} \left(\frac{\hbar}{2NM\omega_{q,p}} \right)^{1/2} \\ \times e^{iq \cdot R_j} (a^+_{q,p} + a_{-q,p}) | \beta \rangle \\ \times \int \psi^*_{k'} \hat{p}_j \cdot \nabla V(r - R_j)\, \psi_k d^3 r, \end{aligned} \tag{A5}$$

where N is the number of ions, M is the ion mass, and $\omega_{q,p}$ is the frequency of the phonon mode (q, p). The phonon part of matrix element vanishes unless the initial and final states differ in the occupation number of the mode (q, p) by unity. In particular, if we take the process in which one particular phonon of (q, p) is emitted by an electron, we have

$$\begin{aligned} M_{\rm ep} = \sum_j \langle n_{q,p} | - i \left(\frac{\hbar}{2NM\omega_{q,p}} \right)^{1/2} \\ \times e^{iq \cdot R_j} (a^+_{q,p} a_{-q,p}) | n_{q,p} - 1 \rangle \end{aligned}$$

$$\times \int \psi^*_{k'} \hat{p}_j \cdot \nabla V(r - R_j) \psi_k d^3 r$$

$$= \sum_j -i \left(\frac{\hbar n_{q,p}}{2NM\omega_{q,p}} \right)^{1/2} e^{iq \cdot R_j}$$

$$\times \int \psi^*_{k'} \hat{p}_j \cdot \nabla V(r - R_j) \psi_k d^3 r, \qquad \text{(A6)}$$

where $|n_{q,p}\rangle$ denotes the state in which there is $n_{q,p}$ phonons of mode $(q, p$; the occupation numbers for all the other phonon modes are omitted for brevity). Note that q and p now denote the wave vector and the polarization of specific phonon mode involved in the electron-phonon coupling and are no longer the running index of summation. Since the phonon part of the matrix element is now constant, the electron-phonon coupling selection rule is dictated by the electronic part of the matrix element

$$\sum_j \int \psi^*_{k'} \hat{p}_j \cdot \nabla V(r - R_j) \psi_k d^3 r. \qquad \text{(A7)}$$

In general, the integral must vanish if the triple tensor product of irreducible representations of initial state, final state and perturbation operator does not contain a fully symmetric representation. In the present study, the band renormalization is observed for the electronic states near the Fermi level along the $\bar{\Gamma} - \bar{X}$ direction, and the symmetry of the associated wave functions were found to be even with respect to the reflection about xz plane (i.e., transforms as A′ representation in the C_{1h} group). Thus, the phonons with the wave vector along the $\bar{\Gamma} - \bar{X}$ direction are allowed to couple with these electrons of A′ symmetry only if the polarization of phonon and the final electronic state share the same symmetry (i.e., both A′ or both A″). In particular, for the coupling with $q = 2k_F$, for which the initial and final electronic states share the same symmetry (A′), we are lead to conclude that the coupling phonons must also have A′ symmetry. Since the horizontal transverse mode (marked brown in Fig. 5) transforms as A,″ it cannot serve as a coupling mode and hence is not expected to contribute to the Eliashberg function or the observed band renormalization (at least for the contribution due to electron-phonon coupling). It is important to note that this selection rule only applies when the initial and final electronic states lie along the same symmetry axis. For any final states at the general point in the SBZ (near the Fermi level), the symmetry selection rule does not *a priori* exclude the possibility of electron-phonon coupling, provided, of course, the existence of phonon modes that conserve the momentum.

[1] G. Grimvall, *The Electron-Phonon Interaction in Metals (Selected Topics in Solid State Physics XVI)*, 1st ed. (North Holland, Amsterdam, 1981).

[2] P. Hofmann, I. Y. Sklyadneva, E. D. L. Rienks, and E. V. Chulkov, New J. Phys. **11**, 125005 (2009).

[3] J. Kroger, Rep. Prog. Phys. **69**, 899 (2006).

[4] M. Hengsberger, D. Purdie, P. Segovia, M. Garnier, and Y. Baer, Phys. Rev. Lett. **83**, 592 (1999).

[5] T. Valla, A. V. Fedorov, P. D. Johnson, and S. L. Hulbert, Phys. Rev. Lett. **83**, 2085 (1999).

[6] T. Balasubramanian, E. Jensen, X. L. Wu, and S. L. Hulbert, Phys. Rev. B **57**, 6866 (1998).

[7] A. Eiguren, S. de Gironcoli, E. V. Chulkov, P. M. Echenique, and E. Tosatti, Phys. Rev. Lett. **91**, 166803 (2003).

[8] S. LaShell, E. Jensen, and T. Balasubramanian, Phys. Rev. B **61**, 2371 (2000).

[9] A. Eiguren, B. Hellsing, E. V. Chulkov, and P. M. Echenique, Phys. Rev. B **67**, 235423 (2003).

[10] A. Eiguren, B. Hellsing, F. Reinert, G. Nicolay, E. V. Chulkov, V. M. Silkin, S. Hüfner, and P. M. Echenique, Phys. Rev. Lett. **88**, 066805 (2002).

[11] B. A. McDougall, T. Balasubramanian, and E. Jensen, Phys. Rev. B **51**, 13891 (1995).

[12] F. Reinert, G. Nicolay, S. Schmidt, D. Ehm, and S. Hüfner, Phys. Rev. B **63**, 115415 (2001).

[13] X. Y. Cui, K. Shimada, M. Hoesch, Y. Sakisaka, H. Kato, Y. Aiura, M. Higashiguchi, Y. Miura, H. Namatame, and M. Taniguchi, Surf. Sci. **601**, 4010 (2007).

[14] X. Y. Cui, K. Shimada, Y. Sakisaka, H. Kato, M. Hoesch, T. Oguchi, Y. Aiura, H. Namatame, and M. Taniguchi, Phys. Rev. B **82**, 195132 (2010).

[15] J. Jiang, M. Higashiguchi, N. Tobida, K. Tanaka, S. Fukuda, H. Hayashi, K. Shimada, H. Namatame, and M. Taniguchi, e-J. Surf. Sci. Nanotechnol. **7**, 57 (2009).

[16] M. Fuglsang Jensen, T. K. Kim, S. Bengió, I. Y. Sklyadneva, A. Leonardo, S. V. Eremeev, E. V. Chulkov, and P. Hofmann, Phys. Rev. B **75**, 153404 (2007).

[17] J. Jiang, K. Shimada, H. Hayashi, H. Iwasawa, Y. Aiura, H. Namatame, and M. Taniguchi, Phys. Rev. B **84**, 155124 (2011).

[18] N. Wu, Y. B. Losovyj, K. Fukutani, and P. A. Dowben, J. Phys.: Condens. Matter **22**, 245501 (2010).

[19] I. Yakovkin and P. A. Dowben, J. Phys.: Condens. Matter **23**, 225503 (2011).

[20] E. Rotenberg and S. Kevan, J. Electron Spectrosc. Relat. Phenom. **126**, 125 (2002).

[21] E. Rotenberg, J. Schaefer, and S. D. Kevan, Phys. Rev. Lett. **84**, 2925 (2000).

[22] K. Fukutani, H. Hayashi, I. N. Yakovkin, T. R. Paudel, T. Habuchi, D. Hirayama, J. Jiang, H. Iwasawa, K. Shimada, N. Wu, E. Y. Tsymbal, Y. B. Losovyj, and P. A. Dowben, Phys. Rev. B **85**, 155435 (2012).

[23] K. Fukutani, N. Lozova, S. M. Zuber, P. A. Dowben, P. Galiy, and Y. B. Losovyj, Appl. Surf. Sci. **256**, 4796 (2010).

[24] K. Shimada, M. Arita, Y. Takeda, H. Fujino, K. Kobayashi, T. Narimura, H. Namatame, and M. Taniguchi, Surf. Rev. Lett. **9**, 529 (2002).

[25] T. McAvoy, J. Zhang, C. Waldfried, D. McIlroy, P. A. Dowben, O. Zeybek, T. Bertrams, and S. Barrett, Eur. Phys. J. B **14**, 747 (2000).

[26] I. N. Yakovkin, J. Zhang, and P. A. Dowben, Phys. Rev. B **63**, 115408 (2001).

[27]H. K. Jeong, T. Komesu, I. N. Yakovkin, and P. A. Dowben, Surf. Sci. Lett. **494**, L773 (2001).
[28]N. Wu, Y. B. Losovyj, Z. Yu, R. F. Sabirianov, W. N. Mei, N. Lozova, J. A. Colón Santana, and P. A. Dowben, J. Phys.: Condens. Matter **21**, 474222 (2009).
[29]K. Fukutani, Y. B. Losovyj, N. Lozova, I. N. Yakovkin, N. Wu, and P. A. Dowben, J. Electron Spectrosc. Relat. Phenom. **184**, 318 (2011).
[30]T. Gallon and J. Matthew, Rev. Phys. Technol. **3**, 31 (1972).
[31]J. P. Perdew, K. Burke, and M. Ernzerhof, Phys. Rev. Lett. **77**, 3865 (1996).
[32]X. Gonze, J.-M. Beuken, R. Caracas, F. Detraux, M. Fuchs, G.-M. Rignanese, L. Sindic, M. Verstraete, G. Zerah, F. Jollet, M. Torrent, A. Roy, M. Mikami, Ph. Ghosez, J.-Y. Raty, and D. C. Allan, Comput. Mater. Sci. **25**, 478 (2002).
[33]N. Troullier and J. L. Martins, Phys. Rev. B **43**, 1993 (1991).
[34]S. Y. Savrasov and D. Y. Savrasov, Phys. Rev. B **54**, 16487 (1996).
[35]J. Hermanson, Solid State Commun. **22**, 9 (1977).
[36]H. Bruus and K. Flensberg, *Many-Body Quantum Theory in Condensed Matter Physics: An Introduction* (Oxford University Press, New York, 2004).
[37]M. Higashiguchi, K. Shimada, M. Arita, Y. Miura, N. Tobita, X. Cui, Y. Aiura, H. Namatame, and M. Taniguchi, Surf. Sci. **601**, 4005 (2007).
[38]C. Hodges and J. Wilkins, Phys. Rev. B **4**, 302 (1971).
[39]J. M. Ziman, *Electrons and Phonons: The Theory of Transport Phenomena in Solids* (Oxford University Press, New York, 2001).